

# A MOVING KRIGING MESHFREE METHOD FOR THE VIBRATION ANALYSIS OF HOMOGENOUS MAGNETO-ELECTRO-ELASTIC PLATES

Lieu B. NGUYEN<sup>1</sup>, Chien H. THAI<sup>2,3,\*</sup>, H. NGUYEN-XUAN<sup>4,\*</sup>

<sup>1</sup>Faculty of Civil Engineering, Ho Chi Minh City University of Technology and Education (HCMUTE), Ho Chi Minh City, Vietnam

<sup>2</sup>Division of Computational Mechanics, Institute for Computational Science, Ton Duc Thang University, Ho Chi Minh City, Vietnam

<sup>3</sup>Faculty of Civil Engineering, Ton Duc Thang University, Ho Chi Minh City, Vietnam

<sup>4</sup>CIRTECH Institute, HUTECH University, Ho Chi Minh City, Vietnam

\*Corresponding Authors: Chien H. THAI (Email: thaihoangchien@tdtu.edu.vn) and H. NGUYEN-XUAN (Email: ngx.hung@hutech.edu.vn)

(Received: 13-Feb-2023; accepted: 13-Mar-2023; published: 31-Mar-2023)

DOI: <http://dx.doi.org/10.55579/jaec.202371.397>

**Abstract.** *The free vibration analysis of the homogenous magneto-electro-elastic (MEE) plate based on a refined first-order shear deformation theory and moving Kriging meshfree method is presented in this paper. The refined first-order shear deformation theory (RFSDT) only includes four variables and reduces one variable when compared to the original first-order shear deformation theory. The MEE materials which are coupled between piezoelectric and piezomagnetic effects are combined with BaTiO<sub>3</sub> and CoFe<sub>2</sub>O<sub>4</sub> materials. The magnetic and electric potentials satisfying the Maxwell equations are assumed to be a combination of cosine and linear variations along the plate thickness. The coupled governing equations of motion of the MEE plates are obtained by using the principle of extended virtual displacement. These equations are solved to achieve the natural frequency of MEE plates by utilizing the moving Kriging mesh-free method. Several numerical examples are examined to evaluate the influence of the geometrical parameter on the natural frequency of the MEE plates.*

## Keywords

*Magneto-electric-elastic functionally graded plates, moving Kriging meshfree method, free vibration, refined first-order shear deformation theory.*

## 1. Introduction

In recent years, thanks to the capacity to convert energy from one form to another, magneto electro-elastic (MEE) materials have had a wide range of applications in various industries, including sensors, actuators, energy harvesting, medical devices, and aerospace and defense. MEE materials are a kind of smart materials that show a strong coupling between their magnetic, electric, and elastic properties. In addition, these smart materials have exhibited several advantageous properties such as multi-functional behavior, high sensitivity, low power consumption, tailorable properties, and large deformation. In this study, the MEE materials are created by a combination of the piezoelectric and

piezomagnetic phases from barium titanate (BaTiO<sub>3</sub>) [1] and the cobalt ferrite (CoFe<sub>2</sub>O<sub>4</sub>) [2, 3], respectively.

The study of MEE structures has been concerned by many scientists. Liu et al. [4] and [5] respectively presented the free vibration and bending analyses of an isotropic MEE plate based on a classical plate theory (CPT). In another work, Shooshtari and Razavi [6] studied a free vibration behavior of the laminated MEE rectangular plates under the Pasternak foundation by using the first-order shear deformation theory (FSDT). Similar to this theory, the nonlinear bending analysis of MEE plates was introduced by Chen and Wu [7], Milazzo [8] and Alaimo et al. [9]. On the other hand, Vinyas and Kattimani [10] investigated the vibration response of the MEE plates in hygrothermal environment using the higher-order shear deformation theory (HSDT). The same with this model, the free vibration behavior of carbon nanotube-reinforced MEE plates was provided in [11, 12]. Zheng et al. [13] and Xu et al. [14] investigated the nonlinear bending and vibration behaviors of MEE plates, respectively. Besides, Chen et al. [15] presented the free vibration analysis of MEE-FG plates using a three-dimensional elasticity theory. By using this theory, Zhang et al. [16] investigated static and dynamic behaviors of MEE plates. The bending behavior of FG MEE sandwich plates was also investigated by Pan et al. [17].

As we have known, the solution of such problems using a three-dimensional elasticity theory is not often simple due to complex geometries, large computational costs and other disadvantaged multiple factors. So, the development and use of numerical methods have always been paid attention by scientists. There are several popular methods such as isogeometric analysis (IGA), finite element methods (FEM), meshfree methods, . . . Among them, meshless methods have proven their power in solving various problems. Because they involve uncomplicated dispensation, arbitrary node distribution, and flexibility of placing nodes at random locations. It means that the approximate functions of the meshfree method use only nodal data in the global Cartesian coordinates and the results of displacement and stresses are also immedi-

ately computed at arbitrary points in physical space. This thing is different from IGA/FEM [18, 19, 20] which the calculation is performed in the natural coordinate. In addition, when using the moving Kriging (MK) meshfree method the enforcement of necessary boundary conditions is easily operated similar to FEM. Because the moving Kriging integration shape function satisfies the Kronecker delta function property, it has got huge benefits in enforcing the essential boundary conditions without any special techniques as the penalty methods or Lagrange multiplier of other meshfree methods. Gu [21] has first presented the moving Kriging interpolation and has successfully shown the helpfulness of the MK interpolation functions in solving the two-dimensional boundary value problems. The MK mesh-free method has effectively been utilized for various problems. For example, the static, dynamic and buckling analyses of FG isotropic and sandwich plates based on a two-variable refined plate theory and the higher order shear deformation theory (HSDT) are respectively introduced in [22, 23]. Based on same method, the size-dependent model for analysis of functionally graded carbon nanotube-reinforced composite nanoplates and functionally graded isotropic and sandwich microplates were respectively investigated in Refs. [24, 25]. The nonlinear static bending and free vibration of the FGM plates using an improved MK meshfree method based on a refined plate theory were presented by Nguyen et al. [26]. On the other hand, the local weak-form MK meshfree method was established for two-dimensional structural examination by Lam et al. [27]. Its more enlargements can be obtained in [28, 29]. As we see in the above publications, there is no study of the free vibration of the MEE plates using the MK meshfree method. For those motivations, we utilize the MK meshfree method and a refined first-order shear deformation theory for free vibration analyses of the homogeneous MEE plate. It can be seen that this report is a novel topic and has not been issued yet. The effect of the geometrical parameters on the natural frequency of the homogeneous MEE plate is presented and discussed.

## 2. The Basic Equations

### 2.1. Material properties of the homogeneous MEE plate

A homogeneous MEE plate (length  $a$ , width  $b$  and thickness  $h$ ) subjected to an electric potential  $\Phi(x, y, z, t)$  and magnetic potential  $\Psi(x, y, z, t)$  is considered, as shown in Figure 1. The MEE materials is made by BaTiO<sub>3</sub> and CoFe<sub>2</sub>O<sub>4</sub> materials. Table 1 presents the material properties of a homogeneous MEE square plate.

**Tab. 1:** Material properties of BaTiO<sub>3</sub>-CoFe<sub>2</sub>O<sub>4</sub>.

Elastic (GPa)	$c_{11} = c_{22} = 226; c_{12} = 125; c_{13} = 124; c_{44} = c_{55} = 44.2; c_{66} = 50.5$
Piezoelectric (C/m <sup>2</sup> )	$e_{31} = e_{32} = -2.2; e_{33} = 9.3; e_{15} = 5.8$
Dielectric (10 <sup>-9</sup> C/V.m)	$k_{11} = k_{22} = 5.64; k_{33} = 6.35$
Piezomagnetic (N/A.m)	$q_{15} = q_{24} = 275; q_{31} = q_{32} = 290.1; q_{33} = 349.9$
Magnetolectric (10 <sup>-12</sup> Ns/VC)	$d_{11} = d_{22} = 5.367; d_{33} = 2737.5$
Magnetic (10 <sup>-6</sup> Ns <sup>2</sup> /C <sup>2</sup> )	$\mu_{11} = \mu_{22} = -297; \mu_{33} = 83.5$

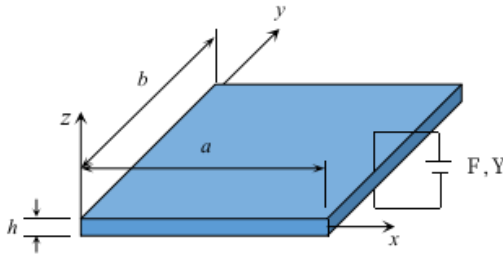


**Fig. 1:** The geometry of MEE rectangular plate.

### 2.2. The refined FSDT formulation

The displacement fields of the MEE plate at any point according to the refined FSDT are presented as follows

$$\hat{u} = \begin{Bmatrix} \hat{u}(x, y, z) \\ \hat{v}(x, y, z) \\ \hat{w}(x, y, z) \end{Bmatrix} = \begin{Bmatrix} u(x, y) \\ v(x, y) \\ w^b(x, y) + w^s(x, y) \end{Bmatrix} - z \begin{Bmatrix} w_{,x}^b(x, y) \\ w_{,y}^b(x, y) \\ 0 \end{Bmatrix} = \mathbf{u}^1(x, y) + z \mathbf{u}^2(x, y) \quad (1)$$

where  $u, v$  are the in-plane displacements along  $x$  and  $y$  directions, respectively;  $w^b$  and  $w^s$  are

transverse bending and shear displacements, respectively. According to the displacement fields in Eq. (1), the linear strain tensor is formulated by

$$\boldsymbol{\varepsilon} = \begin{Bmatrix} \boldsymbol{\varepsilon}^b \\ \boldsymbol{\gamma} \end{Bmatrix} = \begin{Bmatrix} \boldsymbol{\varepsilon}^{b1} + z\boldsymbol{\varepsilon}^{b2} \\ \boldsymbol{\varepsilon}^s \end{Bmatrix} \quad (2)$$

where

$$\boldsymbol{\varepsilon}^b = \begin{Bmatrix} \varepsilon_x \\ \varepsilon_y \\ \gamma_{xy} \end{Bmatrix}; \boldsymbol{\varepsilon}^{b1} = \begin{Bmatrix} u_{,x} \\ v_{,y} \\ u_{,y} + v_{,x} \end{Bmatrix}; \boldsymbol{\varepsilon}^{b2} = - \begin{Bmatrix} w_{,xx}^b \\ w_{,yy}^b \\ 2w_{,xy}^b \end{Bmatrix}; \quad (3)$$

$$\boldsymbol{\gamma} = \begin{Bmatrix} \gamma_{xz} \\ \gamma_{yz} \end{Bmatrix}; \boldsymbol{\varepsilon}^s = \begin{Bmatrix} w_{,x}^s \\ w_{,y}^s \end{Bmatrix}$$

In this study, the electric and magnetic potentials are chosen to satisfy Maxwell's equation and given [30]

$$\Phi(x, y, z) = g(z) \varphi(x, y) + \frac{2z}{h} \varphi_0; \quad (4)$$

$$\Psi(x, y, z) = g(z) \psi(x, y) + \frac{2z}{h} \psi_0$$

where  $\Phi$  and  $\Psi$  are the electric and magnetic potentials, respectively;  $\phi_0$  and  $\psi_0$  are initial electric voltage and magnetic potential, respectively;  $g(z) = -\cos(\pi z/h)$ . The electric ( $\mathbf{E}$ ) and magnetic ( $\mathbf{H}$ ) fields according to Eq. (4) can be formulated by

$$\mathbf{E} = \begin{Bmatrix} E_x \\ E_y \\ E_z \end{Bmatrix} = - \begin{Bmatrix} \Phi_{,x} \\ \Phi_{,y} \\ \Phi_{,z} \end{Bmatrix} = - \begin{Bmatrix} g(z) \varphi_{,x} \\ g(z) \varphi_{,y} \\ g'(z) \varphi + 2\varphi_0/h \end{Bmatrix}; \quad (5)$$

$$\mathbf{H} = \begin{Bmatrix} H_x \\ H_y \\ H_z \end{Bmatrix} = - \begin{Bmatrix} \Psi_{,x} \\ \Psi_{,y} \\ \Psi_{,z} \end{Bmatrix} = - \begin{Bmatrix} g(z) \psi_{,x} \\ g(z) \psi_{,y} \\ g'(z) \psi + 2\psi_0/h \end{Bmatrix}$$

### 2.3. Constitutive equations

For the analysis of the MEE plate, the couple constitutive equations are presented by

$$\begin{aligned} \begin{Bmatrix} \sigma_x \\ \sigma_y \\ \tau_{xy} \\ \tau_{xz} \\ \tau_{yz} \end{Bmatrix} &= \begin{bmatrix} \tilde{c}_{11} & \tilde{c}_{12} & 0 & 0 & 0 \\ \tilde{c}_{12} & \tilde{c}_{22} & 0 & 0 & 0 \\ 0 & 0 & \tilde{c}_{66} & 0 & 0 \\ 0 & 0 & 0 & \tilde{c}_{44} & 0 \\ 0 & 0 & 0 & 0 & \tilde{c}_{55} \end{bmatrix} \begin{Bmatrix} \varepsilon_x \\ \varepsilon_y \\ \gamma_{xy} \\ \gamma_{xz} \\ \gamma_{yz} \end{Bmatrix} - \dots \\ \begin{bmatrix} 0 & 0 & \tilde{e}_{31} \\ 0 & 0 & \tilde{e}_{31} \\ 0 & 0 & 0 \\ \tilde{e}_{15} & 0 & 0 \\ 0 & \tilde{e}_{15} & 0 \end{bmatrix} \begin{Bmatrix} E_x \\ E_y \\ E_z \end{Bmatrix} - \begin{bmatrix} 0 & 0 & \tilde{q}_{31} \\ 0 & 0 & \tilde{q}_{31} \\ 0 & 0 & 0 \\ \tilde{q}_{15} & 0 & 0 \\ 0 & \tilde{q}_{15} & 0 \end{bmatrix} \begin{Bmatrix} H_x \\ H_y \\ H_z \end{Bmatrix}; \\ \begin{Bmatrix} D_x \\ D_y \\ D_z \end{Bmatrix} &= \begin{bmatrix} 0 & 0 & 0 & \tilde{e}_{15} & 0 \\ 0 & 0 & 0 & 0 & \tilde{e}_{15} \\ \tilde{e}_{31} & \tilde{e}_{31} & 0 & 0 & 0 \end{bmatrix} \begin{Bmatrix} \varepsilon_x \\ \varepsilon_y \\ \gamma_{xy} \\ \gamma_{xz} \\ \gamma_{yz} \end{Bmatrix} + \dots \\ \begin{bmatrix} \tilde{k}_{11} & 0 & 0 \\ 0 & \tilde{k}_{22} & 0 \\ 0 & 0 & \tilde{k}_{33} \end{bmatrix} \begin{Bmatrix} E_x \\ E_y \\ E_z \end{Bmatrix} + \begin{bmatrix} \tilde{d}_{11} & 0 & 0 \\ 0 & \tilde{d}_{22} & 0 \\ 0 & 0 & \tilde{d}_{33} \end{bmatrix} \begin{Bmatrix} H_x \\ H_y \\ H_z \end{Bmatrix}; \\ \begin{Bmatrix} B_x \\ B_y \\ B_z \end{Bmatrix} &= \begin{bmatrix} 0 & 0 & 0 & \tilde{q}_{15} & 0 \\ 0 & 0 & 0 & 0 & \tilde{q}_{15} \\ \tilde{q}_{31} & \tilde{q}_{31} & 0 & 0 & 0 \end{bmatrix} \begin{Bmatrix} \varepsilon_x \\ \varepsilon_y \\ \gamma_{xy} \\ \gamma_{xz} \\ \gamma_{yz} \end{Bmatrix} + \dots \\ \begin{bmatrix} \tilde{d}_{11} & 0 & 0 \\ 0 & \tilde{d}_{22} & 0 \\ 0 & 0 & \tilde{d}_{33} \end{bmatrix} \begin{Bmatrix} E_x \\ E_y \\ E_z \end{Bmatrix} + \begin{bmatrix} \tilde{m}_{11} & 0 & 0 \\ 0 & \tilde{m}_{22} & 0 \\ 0 & 0 & \tilde{m}_{33} \end{bmatrix} \begin{Bmatrix} H_x \\ H_y \\ H_z \end{Bmatrix} \end{aligned} \tag{6}$$

in which  $\sigma_x, \sigma_y, \tau_{xy}, \tau_{xz}, \tau_{yz}$  are the stress components;  $D_x, D_y, D_z$  are the electric displacements and  $B_x, B_y, B_z$  are the magnetic inductions;  $\tilde{c}_{ij}$  are symbol of the reduced elastic coefficients;  $\tilde{e}_{ij}$  are the reduced piezo-electric constants;  $\tilde{q}_{ij}$  are the magnetostrictive constants;  $\tilde{k}_{ij}$  are the dielectric coefficients;  $\tilde{d}_{ij}$  and  $\tilde{m}_{ij}$  are the electro-magnetic coupling coefficients and magnetic permittivity coefficients, respectively. The reduced material properties used in Eq. (6) are defined as follows

$$\begin{aligned} \tilde{c}_{11} &= c_{11} - \frac{c_{13}^2}{c_{33}}; \tilde{c}_{12} = c_{12} - \frac{c_{13}c_{23}}{c_{33}}; \tilde{c}_{66} = c_{66}; \tilde{c}_{55} = c_{55}; \\ \tilde{c}_{44} &= c_{44}; \tilde{e}_{31} = e_{31} - \frac{e_{33}c_{13}}{c_{33}}; \tilde{e}_{15} = e_{15}; \tilde{q}_{31} = q_{31} - \frac{q_{33}c_{13}}{c_{33}}; \\ \tilde{q}_{15} &= q_{15}; \tilde{k}_{33} = k_{33} + \frac{e_{33}^2}{c_{33}}; \tilde{k}_{11} = k_{11}; \tilde{d}_{33} = d_{33} + \frac{q_{33}e_{33}}{c_{33}}; \\ \tilde{d}_{11} &= d_{11}; \tilde{m}_{33} = \tilde{m}_{33} + \frac{q_{33}^2}{c_{33}}; \tilde{m}_{11} = m_{11} \end{aligned} \tag{7}$$

For numerical computations, the Eq. (6) can be rewritten by a matrix form as follows

$$\begin{aligned} \begin{Bmatrix} \boldsymbol{\alpha}^b \\ \boldsymbol{\alpha}^s \end{Bmatrix} &= \begin{bmatrix} \mathbf{C}_{uu}^b & \mathbf{0} \\ \mathbf{0} & \mathbf{C}_{uu}^s \end{bmatrix} \begin{Bmatrix} \boldsymbol{\gamma}^b \\ \boldsymbol{\gamma}^s \end{Bmatrix} - \begin{bmatrix} \mathbf{C}_{u\varphi}^b & \mathbf{0} \\ \mathbf{0} & \mathbf{C}_{u\varphi}^s \end{bmatrix} \begin{Bmatrix} \mathbf{E}^b \\ \mathbf{E}^s \end{Bmatrix} - \dots \\ &\begin{bmatrix} \mathbf{C}_{u\psi}^b & \mathbf{0} \\ \mathbf{0} & \mathbf{C}_{u\psi}^s \end{bmatrix} \begin{Bmatrix} \mathbf{H}^b \\ \mathbf{H}^s \end{Bmatrix}; \\ \begin{Bmatrix} \mathbf{D}^b \\ \mathbf{D}^s \end{Bmatrix} &= \begin{bmatrix} \mathbf{C}_{u\varphi}^{bT} & \mathbf{0} \\ \mathbf{0} & \mathbf{C}_{u\varphi}^s \end{bmatrix} \begin{Bmatrix} \boldsymbol{\varepsilon}^b \\ \boldsymbol{\gamma}^s \end{Bmatrix} + \begin{bmatrix} \mathbf{C}_{\varphi\varphi}^b & \mathbf{0} \\ \mathbf{0} & \mathbf{C}_{\varphi\varphi}^s \end{bmatrix} \begin{Bmatrix} \mathbf{s}^b \\ \mathbf{s}^s \end{Bmatrix} + \dots \\ &\begin{bmatrix} \mathbf{C}_{\varphi\psi}^b & \mathbf{0} \\ \mathbf{0} & \mathbf{C}_{\varphi\psi}^s \end{bmatrix} \begin{Bmatrix} \mathbf{H}^b \\ \mathbf{H}^s \end{Bmatrix}; \\ \begin{Bmatrix} \mathbf{B}^b \\ \mathbf{B}^s \end{Bmatrix} &= \begin{bmatrix} \mathbf{C}_{u\psi}^{bT} & \mathbf{0} \\ \mathbf{0} & \mathbf{C}_{u\psi}^s \end{bmatrix} \begin{Bmatrix} \boldsymbol{\varepsilon}^b \\ \boldsymbol{\gamma}^s \end{Bmatrix} + \begin{bmatrix} \mathbf{C}_{\varphi\psi}^b & \mathbf{0} \\ \mathbf{0} & \mathbf{C}_{\varphi\psi}^s \end{bmatrix} \begin{Bmatrix} \mathbf{s}^b \\ \mathbf{s}^s \end{Bmatrix} + \dots \\ &\begin{bmatrix} \mathbf{C}_{\psi\psi}^b & \mathbf{0} \\ \mathbf{0} & \mathbf{C}_{\psi\psi}^s \end{bmatrix} \begin{Bmatrix} \mathbf{H}^b \\ \mathbf{H}^s \end{Bmatrix} \end{aligned} \tag{8}$$

where

$$\begin{aligned} \boldsymbol{\alpha}^b &= \begin{Bmatrix} \sigma_x \\ \sigma_y \\ \tau_{xy} \end{Bmatrix}; \boldsymbol{\alpha}^s = \begin{Bmatrix} \tau_{xz} \\ \tau_{yz} \end{Bmatrix}; \mathbf{D}^b = \begin{Bmatrix} 0 \\ 0 \\ D_z \end{Bmatrix}; \mathbf{D}^s = \begin{Bmatrix} D_x \\ D_y \end{Bmatrix}; \\ \mathbf{B}^b &= \begin{Bmatrix} 0 \\ 0 \\ B_z \end{Bmatrix}; \mathbf{B}^s = \begin{Bmatrix} B_x \\ B_y \end{Bmatrix}; \mathbf{E}^b = \begin{Bmatrix} 0 \\ 0 \\ E_z \end{Bmatrix}; \mathbf{E}^s = \begin{Bmatrix} E_x \\ E_y \end{Bmatrix}; \\ \mathbf{H}^b &= \begin{Bmatrix} 0 \\ 0 \\ H_z \end{Bmatrix}; \mathbf{H}^s = \begin{Bmatrix} H_x \\ H_y \end{Bmatrix}; \end{aligned} \tag{9}$$

in which

$$\begin{aligned} \mathbf{C}_{uu}^b &= \begin{bmatrix} \tilde{c}_{11} & \tilde{c}_{12} & 0 \\ \tilde{c}_{12} & \tilde{c}_{22} & 0 \\ 0 & 0 & \tilde{c}_{66} \end{bmatrix}; \mathbf{C}_{u\varphi}^b = \begin{bmatrix} 0 & 0 & \tilde{e}_{31} \\ 0 & 0 & \tilde{e}_{31} \\ 0 & 0 & 0 \end{bmatrix}; \\ \mathbf{C}_{u\psi}^b &= \begin{bmatrix} 0 & 0 & \tilde{q}_{31} \\ 0 & 0 & \tilde{q}_{31} \\ 0 & 0 & 0 \end{bmatrix}; \mathbf{C}_{uu}^s = \begin{bmatrix} \tilde{c}_{44} & 0 \\ 0 & \tilde{c}_{55} \end{bmatrix}; \\ \mathbf{C}_{u\varphi}^s &= \begin{bmatrix} \tilde{e}_{15} & 0 \\ 0 & \tilde{e}_{15} \end{bmatrix}; \mathbf{C}_{u\psi}^s = \begin{bmatrix} \tilde{q}_{15} & 0 \\ 0 & \tilde{q}_{15} \end{bmatrix}; \\ \mathbf{C}_{\varphi\varphi}^b &= \begin{bmatrix} 0 & 0 & 0 \\ 0 & 0 & 0 \\ 0 & 0 & \tilde{k}_{33} \end{bmatrix}; \mathbf{C}_{\varphi\psi}^b = \begin{bmatrix} 0 & 0 & 0 \\ 0 & 0 & 0 \\ 0 & 0 & \tilde{d}_{33} \end{bmatrix}; \\ \mathbf{C}_{\psi\psi}^b &= \begin{bmatrix} 0 & 0 & 0 \\ 0 & 0 & 0 \\ 0 & 0 & \tilde{m}_{33} \end{bmatrix}; \mathbf{C}_{\varphi\varphi}^s = \begin{bmatrix} \tilde{k}_{11} & 0 \\ 0 & \tilde{k}_{22} \end{bmatrix}; \\ \mathbf{C}_{\varphi\psi}^s &= \begin{bmatrix} \tilde{d}_{11} & 0 \\ 0 & \tilde{d}_{22} \end{bmatrix}; \mathbf{C}_{\psi\psi}^s = \begin{bmatrix} \tilde{m}_{11} & 0 \\ 0 & \tilde{m}_{22} \end{bmatrix} \end{aligned} \tag{10}$$

### 2.4. Variational equation of equilibrium

According to Hamilton's principle, governing equations of the MEE plate are presented by

$$\int_0^t (\delta\Pi + \delta K - \delta W) dt = 0 \quad (11)$$

where  $\delta\Pi$ ,  $\delta K$  and  $\delta W$  are the virtual strain energy, virtual kinetic energy and virtual work done by external electric voltage and magnetic potential, respectively. The virtual strain energy of the MEE plate is defined by

$$\delta\Pi = \int_V \left( \delta(\bar{\boldsymbol{\sigma}}^b)^T \boldsymbol{\alpha}^b + \delta\gamma^T \boldsymbol{\alpha}^s - \delta(\mathbf{E}^b)^T \mathbf{D}^b - \dots \right) dV \quad (12)$$

Substituting Eq. (8) into Eq. (12), the virtual strain energy is reformed by following

$$\begin{aligned} \delta\Pi = & \int_{\Omega} \delta(\bar{\boldsymbol{\sigma}}^b)^T [ \bar{D}_{uu}^b \bar{\boldsymbol{\sigma}}^b - \bar{D}_{u\varphi}^b \bar{\mathbf{E}}^b - \bar{D}_{u\psi}^b \bar{\mathbf{H}}^b ] d\Omega + \dots \\ & \int_{\Omega} \delta(\bar{\boldsymbol{\sigma}}^s)^T [ \bar{D}_{uu}^s \bar{\boldsymbol{\sigma}}^s - \bar{D}_{u\varphi}^s \bar{\mathbf{E}}^s - \bar{D}_{u\psi}^s \bar{\mathbf{H}}^s ] d\Omega - \dots \\ & \int_{\Omega} \delta(\bar{\mathbf{E}}^b)^T [ (\bar{D}_{u\varphi}^b)^T \bar{\boldsymbol{\sigma}}^b + \bar{D}_{\varphi\varphi}^b \bar{\mathbf{E}}^b + \bar{D}_{\varphi\psi}^b \bar{\mathbf{H}}^b ] d\Omega - \dots \\ & \int_{\Omega} \delta(\bar{\mathbf{E}}^s)^T [ (\bar{D}_{u\varphi}^s)^T \bar{\boldsymbol{\sigma}}^s + \bar{D}_{\varphi\varphi}^s \bar{\mathbf{E}}^s + \bar{D}_{\varphi\psi}^s \bar{\mathbf{H}}^s ] d\Omega - \dots \\ & \int_{\Omega} \delta(\bar{\mathbf{H}}^b)^T [ (\bar{D}_{u\psi}^b)^T \bar{\boldsymbol{\sigma}}^b + (\bar{D}_{\varphi\psi}^b)^T \bar{\mathbf{E}}^b + \bar{D}_{\psi\psi}^b \bar{\mathbf{H}}^b ] d\Omega - \dots \\ & \int_{\Omega} \delta(\bar{\mathbf{H}}^s)^T [ (\bar{D}_{u\psi}^s)^T \bar{\boldsymbol{\sigma}}^s + (\bar{D}_{\varphi\psi}^s)^T \bar{\mathbf{E}}^s + \bar{D}_{\psi\psi}^s \bar{\mathbf{H}}^s ] d\Omega \end{aligned} \quad (13)$$

where

$$\bar{\boldsymbol{\sigma}}^b = \{ \varepsilon^{b1} \quad \varepsilon^{b2} \}^T; \bar{\mathbf{E}}^b = \{ 0 \quad 0 \quad \varphi \}^T; \bar{\mathbf{E}}^s = \{ \varphi, x \quad \varphi, y \}^T;$$

$$\bar{\mathbf{H}}^b = \{ 0 \quad 0 \quad \psi \}^T; \bar{\mathbf{H}}^s = \{ \psi, x \quad \psi, y \}^T; \quad (14)$$

$$\bar{D}_{uu}^b = \begin{bmatrix} A^b & B^b \\ B^b & D^b \end{bmatrix}; (A^b, B^b, D^b) = \int_{-h/2}^{h/2} (1, z, z^2) \mathbf{C}_{uu}^b dz;$$

$$\bar{D}_{uu}^s = \int_{-h/2}^{h/2} \mathbf{C}_{uu}^s dz; \bar{\mathbf{D}}_{u\varphi}^b = \{ \hat{\mathbf{C}}_{u\varphi}^{b1} \quad \hat{\mathbf{C}}_{u\varphi}^{b2} \};$$

$$(\hat{\mathbf{C}}_{u\varphi}^{b1}, \hat{\mathbf{C}}_{u\varphi}^{b2}) = \int_{-h/2}^{h/2} \mathbf{C}_{u\varphi}^b(1, z) g'(z) dz; \bar{\mathbf{D}}_{u\varphi}^s = \int_{-h/2}^{h/2} \mathbf{C}_{u\varphi}^s g(z) dz;$$

$$\bar{\mathbf{D}}_{u\psi}^b = \{ \hat{\mathbf{C}}_{u\psi}^{b1} \quad \hat{\mathbf{C}}_{u\psi}^{b2} \}; (\hat{\mathbf{C}}_{u\psi}^{b1}, \hat{\mathbf{C}}_{u\psi}^{b2}) = \int_{-h/2}^{h/2} \mathbf{C}_{u\psi}^b(1, z) g'(z) dz;$$

$$\bar{\mathbf{D}}_{u\psi}^s = \int_{-h/2}^{h/2} \mathbf{C}_{u\psi}^s g(z) dz;$$

$$\bar{\mathbf{D}}_{\varphi\varphi}^b = \int_{-h/2}^{h/2} \mathbf{C}_{\varphi\varphi}^b g'^2(z) dz; \bar{\mathbf{D}}_{\varphi\varphi}^s = \int_{-h/2}^{h/2} \mathbf{C}_{\varphi\varphi}^s g^2(z) dz;$$

$$\bar{\mathbf{D}}_{\varphi\psi}^b = \int_{-h/2}^{h/2} \mathbf{C}_{\varphi\psi}^b g'^2(z) dz; \bar{\mathbf{D}}_{\varphi\psi}^s = \int_{-h/2}^{h/2} \mathbf{C}_{\varphi\psi}^s g^2(z) dz;$$

$$\bar{\mathbf{D}}_{\psi\psi}^b = \int_{-h/2}^{h/2} \mathbf{C}_{\psi\psi}^b g'^2(z) dz; \bar{\mathbf{D}}_{\psi\psi}^s = \int_{-h/2}^{h/2} \mathbf{C}_{\psi\psi}^s g^2(z) dz$$

The virtual kinetic energy is formulated by

$$\delta K = \int_{\Omega} \delta \bar{\mathbf{u}}^T \mathbf{m} \ddot{\mathbf{u}} d\Omega \quad (15)$$

where

$$\bar{\mathbf{u}} = \begin{Bmatrix} \mathbf{u}^1 \\ \mathbf{u}^2 \end{Bmatrix}; \mathbf{m} = \begin{bmatrix} \mathbf{I}_m & 0 \\ 0 & \mathbf{I}_m \end{bmatrix}; \mathbf{I}_m = \begin{bmatrix} I_1 & I_2 \\ I_2 & I_3 \end{bmatrix}; \quad (16)$$

$$(I_1, I_2, I_3) = \int_{-h/2}^{h/2} \rho(z) (1, z, z^2) dz$$

The plate subjected to the pre-buckling forces including the external electric voltage and magnetic potential, the virtual work is given by [30, 31]

$$\delta W = h \int_{\Omega} \delta(B^g)^T \mathbf{N}_0 B^g d\Omega \quad (17)$$

where

$$B^g = \begin{Bmatrix} w_{0,x} \\ w_{0,y} \end{Bmatrix}; \mathbf{N}_0 = \begin{bmatrix} N_x^0 & 0 \\ 0 & N_y^0 \end{bmatrix}; \quad (18)$$

$$N_x^0 = N_x^e + N_x^m; N_y^0 = N_y^e + N_y^m;$$

$$N_x^e = N_y^e = -2\tilde{e}_{31}\varphi_0; N_x^m = N_y^m = -2\tilde{q}_{31}\psi_0$$

Inserting Eqs. (15), (13), and (17) into Eq. (11), the weak form of the MEE plates is reformed as follows

$$\begin{aligned} \delta\Pi = & \int_{\Omega} \delta(\bar{\boldsymbol{\sigma}}^b)^T [ \bar{D}_{uu}^b \bar{\boldsymbol{\sigma}}^b - \bar{D}_{u\varphi}^b \bar{\mathbf{E}}^b - \bar{D}_{u\psi}^b \bar{\mathbf{H}}^b ] d\Omega + \dots \\ & \int_{\Omega} \delta(\bar{\boldsymbol{\sigma}}^s)^T [ \bar{D}_{uu}^s \bar{\boldsymbol{\sigma}}^s - \bar{D}_{u\varphi}^s \bar{\mathbf{E}}^s - \bar{D}_{u\psi}^s \bar{\mathbf{H}}^s ] d\Omega - \dots \\ & \int_{\Omega} \delta(\bar{\mathbf{E}}^b)^T [ (\bar{D}_{u\varphi}^b)^T \bar{\boldsymbol{\sigma}}^b + \bar{D}_{\varphi\varphi}^b \bar{\mathbf{E}}^b + \bar{D}_{\varphi\psi}^b \bar{\mathbf{H}}^b ] d\Omega - \dots \\ & \int_{\Omega} \delta(\bar{\mathbf{E}}^s)^T [ (\bar{D}_{u\varphi}^s)^T \bar{\boldsymbol{\sigma}}^s + \bar{D}_{\varphi\varphi}^s \bar{\mathbf{E}}^s + \bar{D}_{\varphi\psi}^s \bar{\mathbf{H}}^s ] d\Omega - \dots \\ & \int_{\Omega} \delta(\bar{\mathbf{H}}^b)^T [ (\bar{D}_{u\psi}^b)^T \bar{\boldsymbol{\sigma}}^b + (\bar{D}_{\varphi\psi}^b)^T \bar{\mathbf{E}}^b + \bar{D}_{\psi\psi}^b \bar{\mathbf{H}}^b ] d\Omega - \dots \\ & \int_{\Omega} \delta(\bar{\mathbf{H}}^s)^T [ (\bar{D}_{u\psi}^s)^T \bar{\boldsymbol{\sigma}}^s + (\bar{D}_{\varphi\psi}^s)^T \bar{\mathbf{E}}^s + \bar{D}_{\psi\psi}^s \bar{\mathbf{H}}^s ] d\Omega - \dots \\ & h \int_{\Omega} \delta(B^g)^T \mathbf{N}_0 B^g d\Omega + \int_{\Omega} \delta \bar{\mathbf{u}}^T \mathbf{m} \ddot{\mathbf{u}} d\Omega = 0 \end{aligned} \quad (19)$$

### 2.5. A moving Kriging formulation of the MEE plate

Based on the moving Kriging interpolation shape function [21], the displacement fields in Eq. (1) can be interpolated by

$$\mathbf{u}^h(\mathbf{x}) = \sum_{I=1}^N N_I(x, y) I_{6 \times 6} \mathbf{d}_I \quad (20)$$

where N is the total number of nodes in the problem domain; NI is the moving Kriging interpolation shape function; is a unique matrix and is the degree of freedom (DOFs) at a node. Bending and shear components are rewritten by inserting Eq. (20) into Eq. (2) by

$$\boldsymbol{\varepsilon}^b = \{\varepsilon^{b1} \quad \varepsilon^{b2}\}^T = \sum_{I=1}^N \{B_I^{b1} \quad B_I^{b2}\}^T d_I = \sum_{I=1}^N \bar{B}_I^b d_I \quad (21)$$

$$\boldsymbol{\varepsilon}^s = \sum_{I=1}^N \bar{B}_I^s d_I$$

where

$$B_I^{b1} = \begin{bmatrix} N_{I,x} & 0 & 0 & 0 & 0 & 0 \\ 0 & N_{I,y} & 0 & 0 & 0 & 0 \\ N_{I,y} & N_{I,x} & 0 & 0 & 0 & 0 \end{bmatrix}$$

$$B_I^{b2} = - \begin{bmatrix} 0 & 0 & N_{I,xx} & 0 & 0 & 0 \\ 0 & 0 & N_{I,yy} & 0 & 0 & 0 \\ 0 & 0 & 2N_{I,xy} & 0 & 0 & 0 \end{bmatrix} \quad (22)$$

$$\bar{B}_I^s = \begin{bmatrix} 0 & 0 & 0 & N_{I,x} & 0 & 0 \\ 0 & 0 & 0 & N_{I,y} & 0 & 0 \end{bmatrix}$$

Substituting Eq. (20) into Eq. (5), electric and magnetic fields are presented by

$$\mathbf{E}^b = \sum_{I=1}^N \bar{\mathbf{B}}_{\varphi I}^b \mathbf{d}_I; \quad \mathbf{E}^s = \sum_{I=1}^N \bar{\mathbf{B}}_{\varphi I}^s \mathbf{d}_I \quad (23)$$

$$\mathbf{H}^b = \sum_{I=1}^N \bar{\mathbf{B}}_{\psi I}^b d_I; \quad \mathbf{H}^s = \sum_{I=1}^N \bar{\mathbf{B}}_{\psi I}^s d_I$$

where

$$\bar{\mathbf{B}}_{\varphi I}^b = \begin{bmatrix} 0 & 0 & 0 & 0 & 0 & 0 \\ 0 & 0 & 0 & 0 & 0 & 0 \\ 0 & 0 & 0 & 0 & -N_I & 0 \end{bmatrix}$$

$$\bar{\mathbf{B}}_{\psi I}^b = \begin{bmatrix} 0 & 0 & 0 & 0 & 0 & 0 \\ 0 & 0 & 0 & 0 & 0 & 0 \\ 0 & 0 & 0 & 0 & 0 & -N_I \end{bmatrix} \quad (24)$$

$$\bar{\mathbf{B}}_{\varphi I}^s = \begin{bmatrix} 0 & 0 & 0 & 0 & -N_{I,x} & 0 \\ 0 & 0 & 0 & 0 & -N_{I,y} & 0 \end{bmatrix}$$

$$\bar{\mathbf{B}}_{\psi I}^s = \begin{bmatrix} 0 & 0 & 0 & 0 & 0 & -N_{I,x} \\ 0 & 0 & 0 & 0 & 0 & -N_{I,y} \end{bmatrix}$$

Similarly, by substituting Eq. (20) into Eq. (1), displacement fields are expressed by

$$\bar{\mathbf{u}} = \{u^1 \quad u^2\}^T = \sum_{I=1}^N \{M_I^1 \quad M_I^2\}^T d_I = \sum_{I=1}^N \bar{M}_I d_I \quad (25)$$

where

$$M_I^1 = \begin{bmatrix} N_I & 0 & 0 & 0 & 0 & 0 \\ 0 & N_I & 0 & 0 & 0 & 0 \\ 0 & 0 & N_I & N_I & 0 & 0 \end{bmatrix} \quad (26)$$

$$M_I^2 = - \begin{bmatrix} 0 & 0 & N_I & 0 & 0 & 0 \\ 0 & 0 & N_I & 0 & 0 & 0 \\ 0 & 0 & 0 & 0 & 0 & 0 \end{bmatrix}$$

The matrix is described by replacing Eq. (20) with Eq. (17) as follows

$$B^g = \sum_{I=1}^N \bar{\mathbf{B}}_I^g d_I \quad (27)$$

where

$$\bar{\mathbf{B}}_I^g = \begin{bmatrix} 0 & 0 & N_{I,x} & N_{I,x} & 0 & 0 \\ 0 & 0 & N_{I,y} & N_{I,y} & 0 & 0 \end{bmatrix} \quad (28)$$

Finally, the governing equations for the MEE plates are formulated by inserting the corresponding components into Eq. (19) as

$$((K - K_g) - \omega^2 M) \bar{\mathbf{d}} = 0 \quad (29)$$

where  $\mathbf{K}$ ,  $\mathbf{M}$  and  $\mathbf{K}_g$  are the global stiffness matrix, mass matrix, and geometry matrix, respectively, and

$$\mathbf{K} = \int_{\Omega} (\bar{\mathbf{B}}^b)^T \bar{D}_{uu}^b \bar{\mathbf{B}}^b d\Omega - \int_{\Omega} (\bar{\mathbf{B}}^b)^T \bar{D}_{ue}^b \bar{\mathbf{B}}_{\varphi}^b d\Omega - \dots$$

$$\int_{\Omega} (\bar{\mathbf{B}}^b)^T \bar{D}_{um}^b \bar{\mathbf{B}}_{\psi}^b d\Omega + \int_{\Omega} (\bar{\mathbf{B}}^s)^T D_{uu}^s \bar{\mathbf{B}}^s d\Omega - \dots$$

$$\int_{\Omega} (\bar{\mathbf{B}}^s)^T \bar{D}_{ue}^s \bar{\mathbf{B}}_{\varphi}^s d\Omega - \int_{\Omega} (\bar{\mathbf{B}}^s)^T \bar{D}_{um}^s \bar{\mathbf{B}}_{\psi}^s d\Omega - \dots$$

$$\begin{aligned}
 & \int_{\Omega} (\bar{\mathbf{B}}_{\varphi}^b)^T \bar{D}_{eu} \bar{\mathbf{B}}^b d\Omega - \int_{\Omega} (\bar{\mathbf{B}}_{\varphi}^b)^T \bar{D}_{ee}^b \bar{\mathbf{B}}_{\varphi}^b d\Omega - \dots \\
 & \int_{\Omega} (\bar{\mathbf{B}}_{\varphi}^b)^T \bar{D}_{em}^b \bar{\mathbf{B}}_{\psi}^b d\Omega - \int_{\Omega} (\bar{\mathbf{B}}_{\varphi}^s)^T \bar{D}_{eu}^s \bar{\mathbf{B}}^s d\Omega - \dots \\
 & \int_{\Omega} (\bar{\mathbf{B}}_{\varphi}^s)^T \bar{D}_{ee}^s \bar{\mathbf{B}}_{\varphi}^s d\Omega - \int_{\Omega} (\bar{\mathbf{B}}_{\varphi}^s)^T \bar{D}_{em}^s \bar{\mathbf{B}}_{\psi}^s d\Omega - \dots \\
 & \int_{\Omega} (\bar{\mathbf{B}}_{\psi}^b)^T \bar{D}_{mu}^b \bar{\mathbf{B}}^b d\Omega - \int_{\Omega} (\bar{\mathbf{B}}_{\psi}^b)^T \bar{D}_{me}^b \bar{\mathbf{B}}_{\varphi}^b d\Omega - \dots \\
 & \int_{\Omega} (\bar{\mathbf{B}}_{\psi}^b)^T \bar{D}_{mm}^b \bar{\mathbf{B}}_{\psi}^b d\Omega - \int_{\Omega} (\bar{\mathbf{B}}_{\psi}^s)^T \bar{D}_{mu}^s \bar{\mathbf{B}}^s d\Omega - \dots \\
 & \int_{\Omega} (\bar{\mathbf{B}}_{\psi}^s)^T \bar{D}_{me}^s \bar{\mathbf{B}}_{\varphi}^s d\Omega - \int_{\Omega} (\bar{\mathbf{B}}_{\psi}^s)^T \bar{D}_{mm}^s \bar{\mathbf{B}}_{\psi}^s d\Omega \\
 M &= \int_{\Omega} \bar{M}^T m \bar{M} d\Omega; K_g = \int_{\Omega} (\bar{B}^g)^T \mathbf{N}_0 \bar{B}^g d\Omega
 \end{aligned}
 \tag{30}$$

in which  $\omega$  is the natural frequency and  $\bar{\mathbf{d}}$  is the modes shape.

### 3. Numerical Results

In this section, obtained results from the present solution are verified through a numerical example by comparison to published results in the literature. Let us consider a simply supported homogeneous MEE square plate. In this study, the initial electric voltage and magnetic potential are taken by and, respectively. The natural frequency is computed by Table 2 tabulates the four first dimensionless frequencies of the simply supported homogeneous MEE square plate. Obtained results are compared to those reported by Ke et al. [30] using the Kirchhoff plate theory (3DOFs), Sobhy and Mukahal [32] using refined HSDT (4 DOFs), Gholami et al. [33] using HSDT (5 DOFs) and Abazid [34] using refined FSDT (4 DOFs). It is noted that a good agreement between the current and compared results is shown. In addition, it can be seen that obtained results are similar to the results in [34] due to using the same refined FSDT. From these results, it is important that the present solution is accurate and efficient to analyze MEE plates.

Next, the first five non-dimensional natural frequencies of simply supported homogeneous MEE squares with different length-to-thickness ratios are listed in Table 3. It can be seen that

**Tab. 2:** The first four dimensionless natural frequencies  $\bar{\omega}$  of a simply supported MEE square plates (a/h=15).

Refs	$\bar{\omega}$			
	1	2	3	4
Ref [32]	0.3830	0.9330	0.9330	1.4571
Ref [33]	0.3682	0.9136	0.9136	-
Ref [34]	0.3829	0.9329	0.9329	1.4568
Ref [30]	0.3698	0.9247	0.9247	1.4800
Present	0.3843	0.9404	0.9413	1.4757

natural frequencies reduce when increasing the length-to-thickness ratio.

**Tab. 3:** The first five non-dimensional natural frequency  $\bar{\omega} = \omega a \sqrt{\rho/\bar{c}_{11e}}$  of simply supported homogeneous MEE square plates.

a/h	$\bar{\omega}$				
	1	2	3	4	5
5	1.0345	1.7911	1.7917	2.2646	2.2661
10	0.5656	1.3504	1.3516	1.7917	2.0756
20	0.2902	0.7170	0.7177	1.1352	1.4084
50	0.1170	0.2922	0.2925	0.4677	0.5843
100	0.0586	0.1465	0.1467	0.2349	0.2938

Finally, a simply supported MEE-FG square plate with a heart cutout is examined, as shown in Figure 2. Again, as observed, a rise in the length-to-thickness ratio leads to a decline in the natural frequencies of MEE square plates. Moreover, results from MEE square plates with a heart cutout are slightly larger than the ones from MEE square plates. Figure 3 plots the first six modes of shape of the MEE square plates with a heart cutout.

**Tab. 4:** The first five non-dimensional natural frequency  $\bar{\omega} = \omega L \sqrt{\rho/\bar{c}_{11e}}$  of simply supported MEE square plates with a heart cutout.

a/h	$\bar{\omega}$				
	1	2	3	4	5
10	0.6582	1.0199	1.0942	1.2227	1.7833
20	0.3385	0.5729	0.6422	1.0199	1.0324
50	0.1365	0.2325	0.2608	0.4240	0.4647
100	0.0684	0.1165	0.1307	0.2128	0.2334

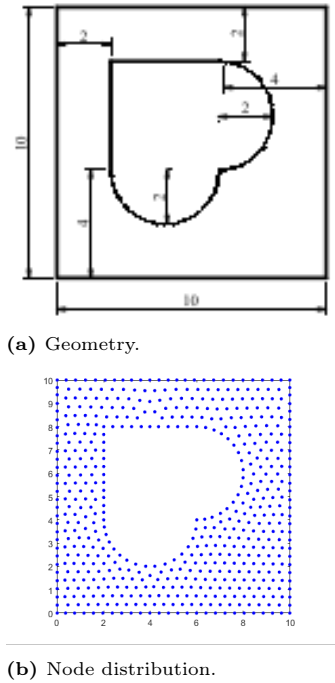


**Fig. 2:** The geometry and node distribution of a square plate with a heart cutout.

## 4. Conclusion

A weak formulation based on the refined FSDT for free vibration analysis of MEE plates was represented in this study by using the principle of extended virtual displacement. Governing equations were also solved by using the moving Kriging mesh-free method to determine the natural frequency of MEE plates. The refined FSDT reduces one variable when compared to the classical FSDT. To satisfy the Maxwell equations, the magnetic and electric potentials are considered by a combination of cosine and linear functions via the plate thickness. Obtained results were compared to the published ones. In this study, it was indicated that the natural frequencies of MEE square plates decrease when increasing the length-to-thickness ratio and are slightly smaller than the ones of MEE square plates with a heart cutout.

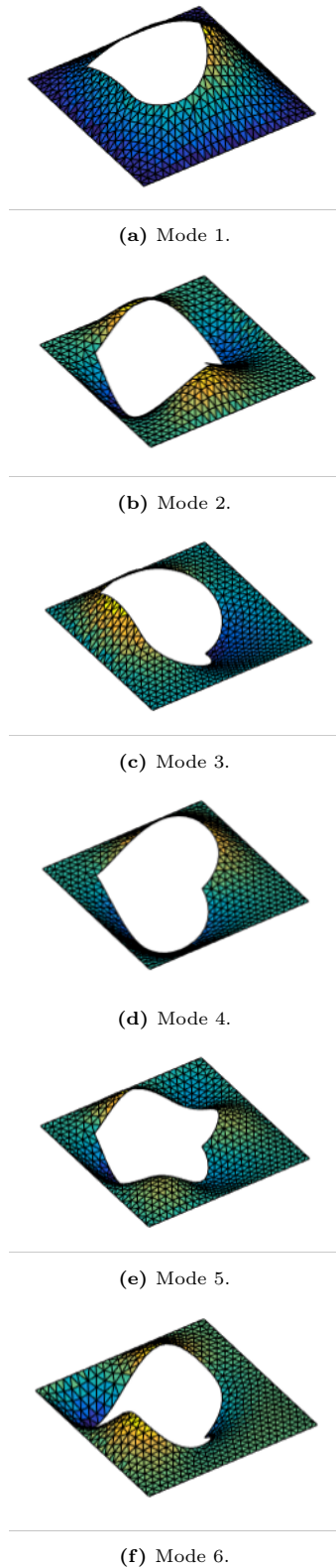


**Fig. 3:** The first six modes shape of the MEE square plates with a heart cutout.

## Acknowledgements

This research is funded by Ho Chi Minh City University of Technology and Education (HCMUTE) under grant number T2022-136.

## References

- [1] Suzuki, K. & Kijima, K. (2005). Optical band gap of barium titanate nanoparticles prepared by RF-plasma chemical vapor deposition. *Japanese journal of applied physics*, 44(4R), 2081.
- [2] Olabi, A.G. & Grunwald, A. (2008). Design and application of magnetostrictive materials. *Materials & Design*, 29(2), 469–483.
- [3] Hosni, N., Zehani, K., Bartoli, T., Besais, L., & Maghraoui-Meherzi, H. (2017). Semi-hard magnetic properties of nanoparticles of cobalt ferrite synthesized by the coprecipitation process. *Journal of Alloys and Compounds*, 694, 1295–1301.
- [4] Liu, M.F. & Chang, T.P. (2010). Closed form expression for the vibration problem of a transversely isotropic magneto-electro-elastic plate.
- [5] Liu, M.F. (2016). Exact solution for the bending deformations of layered magneto-electro-elastic laminates based on thin-plate formulation. *International Journal of Engineering and Applied Sciences*, 3(4), 257692.
- [6] Shoostari, A. & Razavi, S. (2015). Large amplitude free vibration of symmetrically laminated magneto-electro-elastic rectangular plates on Pasternak type foundation. *Mechanics Research Communications*, 69, 103–113.
- [7] Chen, H. & Yu, W. (2014). A multi-physics model for magneto-electro-elastic laminates. *European Journal of Mechanics-A/Solids*, 47, 23–44.
- [8] Milazzo, A. (2014). Large deflection of magneto-electro-elastic laminated plates. *Applied Mathematical Modelling*, 38(5-6), 1737–1752.
- [9] Alaimo, A., Benedetti, I., & Milazzo, A. (2014). A finite element formulation for large deflection of multilayered magneto-electro-elastic plates. *Composite Structures*, 107, 643–653.
- [10] Vinyas, M. & Kattimani, S.C. (2018). Finite element evaluation of free vibration characteristics of magneto-electro-elastic rectangular plates in hygrothermal environment using higher-order shear deformation theory. *Composite Structures*, 202, 1339–1352.
- [11] Vinyas, M. (2019). A higher-order free vibration analysis of carbon nanotube-reinforced magneto-electro-elastic plates using finite element methods. *Composites Part B: Engineering*, 158, 286–301.
- [12] Mahesh, V. & Harursampath, D. (2022). Nonlinear vibration of functionally graded magneto-electro-elastic higher order plates reinforced by CNTs using FEM. *Engineering with Computers*, 38(2), 1029–1051.
- [13] Zheng, Y.f., Xu, L.l., & Chen, C.p. (2021). Nonlinear bending analysis of magneto-electroelastic rectangular plates using higher order shear deformation theory. *Journal of Mechanical Science and Technology*, 35, 1099–1108.
- [14] Xu, L., Kang, C., Zheng, Y., & Chen, C. (2021). Analysis of nonlinear vibration of magneto-electro-elastic plate on elastic foundation based on high-order shear deformation. *Composite Structures*, 271, 114149.
- [15] Chen, W., Lee, K.Y., & Ding, H. (2005). On free vibration of non-homogeneous transversely isotropic magneto-electro-elastic plates. *Journal of Sound and Vibration*, 279(1-2), 237–251.
- [16] Zhang, P., Qi, C., Fang, H., Ma, C., & Huang, Y. (2019). Semi-analytical analysis of static and dynamic responses for laminated magneto-electro-elastic plates. *Composite Structures*, 222, 110933.

- [17] Pan, E. & Han, F. (2005). Exact solution for functionally graded and layered magneto-electro-elastic plates. *International Journal of Engineering Science*, 43(3-4), 321–339.
- [18] Hughes, T.J., Cottrell, J.A., & Bazilevs, Y. (2005). Isogeometric analysis: CAD, finite elements, NURBS, exact geometry and mesh refinement. *Computer methods in applied mechanics and engineering*, 194(39-41), 4135–4195.
- [19] Bazilevs, Y., Takizawa, K., Tezduyar, T.E., Hsu, M.C., Otoguro, Y., Mochizuki, H., & Wu, M.C. (2020). Wind Turbine and Turbomachinery Computational Analysis with the ALE and Space-Time Variational Multiscale Methods and Isogeometric Discretization. *Journal of Advanced Engineering and Computation*, 4(1), 1–32.
- [20] Takizawa, K., Bazilevs, Y., & Tezduyar, T.E. (2022). Mesh moving methods in flow computations with the space-time and arbitrary Lagrangian-Eulerian methods. *J Adv Eng Comput*, 6(85), 112.
- [21] Gu, L. (2003). Moving kriging interpolation and element-free Galerkin method. *International journal for numerical methods in engineering*, 56(1), 1–11.
- [22] Van Do, V.N. & Thai, C.H. (2017). A modified Kirchhoff plate theory for analyzing thermo-mechanical static and buckling responses of functionally graded material plates. *Thin-Walled Structures*, 117, 113–126.
- [23] Thai, C.H., Do, V.N., & Nguyen-Xuan, H. (2016). An improved Moving Kriging-based meshfree method for static, dynamic and buckling analyses of functionally graded isotropic and sandwich plates. *Engineering Analysis with Boundary Elements*, 64, 122–136.
- [24] Thai, C.H., Ferreira, A., Lee, J., & Nguyen-Xuan, H. (2018). An efficient size-dependent computational approach for functionally graded isotropic and sandwich microplates based on modified couple stress theory and moving Kriging-based meshfree method. *International Journal of Mechanical Sciences*, 142, 322–338.
- [25] Thai, C.H., Ferreira, A., Nguyen-Xuan, H., & Phung-Van, P. (2021). A size dependent meshfree model for functionally graded plates based on the nonlocal strain gradient theory. *Composite Structures*, 272, 114169.
- [26] Nguyen, T.N., Thai, C.H., Nguyen-Xuan, H., & Lee, J. (2018). Geometrically nonlinear analysis of functionally graded material plates using an improved moving Kriging meshfree method based on a refined plate theory. *Composite Structures*, 193, 268–280.
- [27] Lam, K., Wang, Q., & Li, H. (2004). A novel meshless approach—Local Kriging (LoKriging) method with two-dimensional structural analysis. *Computational Mechanics*, 33, 235–244.
- [28] Chen, L. & Liew, K.M. (2011). A local Petrov-Galerkin approach with moving Kriging interpolation for solving transient heat conduction problems. *Computational Mechanics*, 47, 455–467.
- [29] Dai, B., Cheng, J., & Zheng, B. (2013). A moving Kriging interpolation-based meshless local Petrov–Galerkin method for elastodynamic analysis. *International Journal of Applied Mechanics*, 5(01), 1350011.
- [30] Ke, L.L., Wang, Y.S., Yang, J., & Kitipornchai, S. (2014). Free vibration of size-dependent magneto-electro-elastic nanoplates based on the nonlocal theory. *Acta Mechanica Sinica*, 30, 516–525.
- [31] Feng, W., Yan, Z., Lin, J., & Zhang, C. (2020). Bending analysis of magneto-electroelastic nanoplates resting on Pasternak elastic foundation based on nonlocal theory. *Applied Mathematics and Mechanics*, 41, 1769–1786.
- [32] Sobhy, M. & Al Mukahal, F. (2022). Analysis of electromagnetic effects on vibration of functionally graded GPLs reinforced piezoelectromagnetic plates on an elastic substrate. *Crystals*, 12(4), 487.

- [33] Gholami, R., Ansari, R., & Gholami, Y. (2017). Size-dependent bending, buckling and vibration of higher-order shear deformable magneto-electro-thermo-elastic rectangular nanoplates. *Materials Research Express*, 4(6), 065702.
- [34] Abazid, M.A. (2019). The nonlocal strain gradient theory for hygrothermo-electromagnetic effects on buckling, vibration and wave propagation in piezo-electromagnetic nanoplates. *International Journal of Applied Mechanics*, 11(07), 1950067.

## About Authors

**Lieu B. NGUYEN** was born in Vietnam in 1984. She has a Ph.D. degree in Engineering Mechanics in 2019. Now, she is a lecturer at the Faculty of Civil Engineering, Ho Chi Minh City University of Technology and Education, Ho Chi Minh City, Vietnam. Her research interests are computational mechanics, and numerical methods for advanced materials.

**Chien H. THAI** received his Ph. D from the University of Science, Viet Nam National University Ho Chi Minh City in 2015. He has been conducting computational mechanics research since 2010. Currently, he is a researcher at Ton Duc Thang University, Ho Chi Minh City, Vietnam. He has published over 70 Web-of-Science-indexed journal articles on computational mechanics.

**H. NGUYEN-XUAN** received his Ph.D. in Computational Mechanics from the University of Liège (Belgium) in 2008. His current research focuses on computational engineering, applied mathematics, data-driven machine learning methodology, 3D printing and hydrogen energy.

Dr. Nguyen-Xuan has carried out significant research collaborations with leading research institutions and universities around the world. The national and international cooperation in research has been providing him widespread recognition in the field of computational mechanics. He has published more than 250 peer-reviewed articles.